Measurement of the self-intermediate scattering function of suspensions of hard spherical particles near the glass transition

W. van Megen, T. C. Mortensen, and S. R. Williams
Department of Applied Physics, Royal Melbourne Institute of Technology, Melbourne, Victoria 3000, Australia

J. Müller*
Institut für Physik, der Johannes-Gutenberg-Universität, Staudingerweg 7, 55099 Mainz, Germany
(Received 4 February 1998; revised manuscript received 25 June 1998)

Dynamic light-scattering measurements are reported for suspensions at concentrations in the vicinity of the glass transition. In a mixture of identically sized but optically different particles having hard-sphere-like interactions, we project out the incoherent (or self-) intermediate scattering functions by adjusting the refractive index of the suspending liquid until scattering from the structure is suppressed. Due to polydispersity, crystallization is sufficiently slow so that good estimates of ensemble-averaged quantities can be measured for the metastable fluid states. Crystallization of the suspensions is still exploited, however, to set the volume fraction scale in terms of effective hard spheres and to eliminate (coherent) scattering from the structure. The glass-transition volume fraction is identified by the value where large-scale particle motion ceases. The nonequilibrium nature of the glass state is evidenced by the dependence on the waiting time of the long time decay of the relaxation functions. The self-intermediate scattering functions show negligible deviation from Gaussian behavior up to the onset of large-scale diffusion in the fluid or the onset of waiting time effects in the glass. [S1063-651X(98)12810-6]

PACS number(s): 64.70.Pf, 61.20.Ne, 82.70.Dd

I. INTRODUCTION

In this paper we present dynamic light-scattering measurements of the self-intermediate scattering functions of concentrated suspensions of colloidal hard spheres. The particle size distribution of the spheres is such that nucleation and crystal growth are sufficiently slow that detailed measurements in the metastable fluids can be made and the glass transition identified.

The propensity for a liquid to vitrify on cooling increases with its molecular complexity. Network forming materials, such as silica, and melts of polymers and salts are examples of liquids that can be cooled at (experimentally attainable) rates that drive them into glassy states. However, simple one-component fluids of spherically symmetrical molecules cannot be cooled sufficiently quickly to bypass crystallization. Recent computer simulations [1] indicate that glasses obtained by means of rapid computer quenches previously considered to be stable [2] are now found to be unstable to crystallization, challenging the notion [3] that even the simplest fluid can in principle be forced into a stable glass provided the quench is fast enough. One exception in that the expected behavior of a quenched system of spherically symmetrical constituents appears to be a colloidal suspension of spherical particles. Previous work [4,5] has shown that suspensions of similarly sized particles with hard-sphere-like interactions show a glass transition (GT) located at the volume fraction $\phi_g \cong 0.575$, where large-scale particle diffusion and crystallization by homogeneous nucleation stop. The value found for ϕ_g is well below the volume fraction ($\phi_r = 0.64$) corresponding to random close packing. Whether or not the colloidal glass ultimately crystallizes and the rate at which it does so are sensitive to the distribution of particle radii [6] as well as gravitational effects [7]. Colloidal glasses composed of particles with an average radius, R, less than about 0.3 μm and with a narrow particle-size distribution (polydispersity less than about 5%) still exhibit some very slow crystal growth seeded by secondary nuclei such as container walls and shear aligned structures induced by the shear-melting process [8,9]. A recent study on a similar suspension of hard-sphere-like particles found the glass to remain so indefinitely on earth but to crystallize in the absence of gravity [7].

Since suspensions of synthetic particles have, for some years, served as valuable experimental models in the study of the glass transition and crystallization [5,10], an important issue to be addressed is the influence of the particle-size distribution on the lifetime of the metastable fluid states, for volume fractions $\phi < \phi_g$, and the stability of the glass. We first reiterate some of the differences between colloidal and simple atomic matter.

Taking the coarse-grained view, a suspension of particles, having radii several thousand times those of atoms, can be regarded as a collection of superatoms moving about in an incompressible fluid. One consequence of this size disparity is that number densities of suspensions are some 10 orders of magnitude smaller than those of atomic materials so that excess thermodynamic properties, such as specific heat (an important indicator in phase-transition studies), are proportionally smaller and, therefore, effectively inaccessible. Correspondingly weak lattice forces allow shear melting of colloidal crystals by applying very modest shear stresses [11]. The diffusive particle motions are also correspondingly

*Present address: Evotec BioSystems, Grandweg 64, 22529 Hamburg, Germany.

slower. This brings crystallization processes into a conveniently accessible time frame. Furthermore, the suspending fluid presents an effective thermal bath. This simplifies crystallization and glass-transition dynamics by removing complications associated with slow dissipation of thermal gradients, which may be generated during crystallization, and effectively suppressing phonon-activated processes, processes purported to be responsible for ergodicity restoration in molecular glasses. In this regard colloidal suspensions are more compatible than molecular systems, with the assumptions upon which classical nucleation theory [12] and mode-coupling theory of the GT [13], for example, are based. Other notable differences are that the suspension volume, rather than pressure, remains fixed during a phase change, and quenched states are produced by shear melting of colloidal crystals. There appears, therefore, to be a tendency for a (density or shear) quenched colloidal fluid to have nonequilibrium structures whose shapes, rather than size, are incompatible with the thermodynamic conditions that pertain in the immediate wake of a quench.

Here we report measurements of self- (or incoherent) intermediate scattering functions (ISF's) in mixtures of polymer and silica particles. These particles have the same average radius and the same hard-sphere-like interactions. Compared with the particles used in previous work [4,5], the polymer particles used in the present experiments have a particle-size distribution (PSD) that is slightly broader and asymmetric. This causes a significant retardation in the nucleation rate (for $\phi<\phi_g$) [6,14], thereby increasing the lifetimes of the metastable colloidal fluid states and facilitating the acquisition of ensemble averages over the particle dynamics in those states. A further consequence of the broader PSD is that crystal growth is completely suppressed in the glass [6] ($\phi>\phi_g$). However, we exploit the fact that at lower volume fractions these suspensions still crystallize, albeit very slowly, in order to define effective (hard-sphere) volume fractions of the samples by identifying the observed freezing-melting transition with that known for hard spheres, and also, since we wish to isolate the self-ISF, to eliminate scattering from the structure.

In this study we also address two further issues raised by previous work. (i) The first is the influence of multiple scattering. Here we overcome this by using a relatively new two-color cross-correlation spectrometer that suppresses multiple scattering [15]. (ii) One might question whether results obtained in one measurement, or compiled from a small number of independent measurements, are truly representative of the ensemble, not just in the glass phase but, perhaps more importantly, in the fluid phase close to the GT where the time scales of the slowest density fluctuations are comparable to the duration of the measurement. These concerns are essentially eliminated by techniques employed here that provide efficient sampling of large numbers of independent spatial Fourier components of the density fluctuations.

This paper is arranged as follows. Experimental methods, described in the following section, comprise a description of the properties and preparation of the samples, the methods used to measure the self-ISF's, the multiple scattering suppression spectrometer, and the procedures by which ensemble-averaged ISF's are obtained. Results are presented and discussed in Sec. III, where we describe the wave-vector dependence of the measured ISF's and the particle mean-squared displacements. Results are also discussed in relation to mode-coupling theory of the GT. Finally, conclusions are presented in Sec. IV.

TABLE I. Average particle radii and polydispersities. See text for details of the particle size distribution.

Species	Radius (nm)	Polydispersity
Silica	200	0.02
Polymer	200	0.06

II. EXPERIMENTAL METHODS

A. Sample description

The suspensions comprise mixtures of polymer particles (98% of total particle volume) and silica particles (2%) suspended in *cis*-decalin. Importantly, both particle types have nearly the same average radius (Table I) and they are sterically stabilized by the same coating of poly-12-hydroxystearic acid of thickness about 10 nm [16]. However, the polymer particles differ from those used in previous work [4,5,16] in two respects.

First, the cores of the polymer particles are composed of a copolymer of methylmethacrylate and trifluoroethylacrylate [*p*-(MMA/TFEA)]. Inclusion of TFEA (at 24% of the total polymer weight) slightly lowers the refractive index of the particles, relative to those of pure *p*-MMA used previously. As a consequence, suspensions of copolymer particles at any concentration are transparent in *cis*-decalin. Furthermore, the suspension's turbidity can be tuned quite finely by varying the temperature [17]. Suspensions of particles with cores of pure *p*-MMA are generally too opaque for light-scattering experiments without the addition of a second solvent with a refractive index that is greater than that of decalin [16,17].

Second, the PSD of the polymer particles, as prepared in the polymerization of MMA and TFEA, is slightly broader and negatively skewed; we find that the wave-vector dependence of the scattered intensity and the diffusion coefficient, measured on dilute suspensions, can be reconciled with a PSD approximated by the sum of two Gaussian distributions with average radii 207 and 176 nm, amplitudes 1 and 0.2, respectively, and the same polydispersity of 0.045 [18,19]. One can therefore regard the suspension of the polymer particles, albeit simplistically, as a bimodal system of hard spheres with radii in the ratio $\gamma=176/207=0.85$ and number fraction X of large spheres of 0.83.

Recent crystallization studies on bimodal suspensions of colloidal hard spheres with $\gamma=0.83$ [14] found that, due possibly to partitioning of the species on solidification, nucleation slows rapidly when X is deceased only slightly from unity. Accordingly, we infer that the slow crystallization rates, which we find here to be at least 10^3 times slower than structural relaxation rates, are due to the finite spread of particle radii. This property of the suspensions is obviously important as far as the experimental viability of the metastable fluid and glass formation are concerned. While a small distribution of particle radii has a dramatic effect on crystallization, ISF's are barely affected [14]. This lends justification to drawing comparisons between the relaxation functions

measured on these polydisperse suspensions and those predicted for ideal one-component systems.

Despite the slow crystallization, in samples with net volume fractions between the freezing and melting values, coexisting colloidal fluid and crystal phases can still be clearly delineated when they are left undisturbed for several days [6]. Thus, as described elsewhere [8,20], in order to take account of the finite range of the solvated steric layer, sample volume fractions ϕ are expressed in effective hard-sphere terms by identifying the observed freezing concentration with the freezing volume fraction, $\phi_f = 0.494$, of a system of perfectly identical hard spheres [21]. (However, see [22].)

Samples were prepared at the required volume fractions, $0.4 \leqslant \phi \leqslant 0.6$, in cylindrical glass cells of 1 cm diam, using procedures described previously [4,16]. We mention only that samples are effectively quenched by tumbling them on a rotary vortex mixer for about one day. This process not only disperses the particles but, as already mentioned, shear melts any crystals that may be present.

B. Dynamic light scattering: Self-intermediate scattering functions

In order to obtain the self- (incoherent) intermediate scattering function from light-scattering measurements, we require a suspension of particles that have a distribution of scattering amplitudes. The refractive indices of the particles and/or solvent must then be adjusted until the average scattering amplitude is zero.

As described in Sec. II A, we use a mixture of polymer and silica (2% by volume) particles. Both particle types carry the same stabilizer and, as far as can be ascertained by DLS, they have the same average radius (Table I). As argued elsewhere [24], one expects, as a result of the range ($\approx$10 nm) of the steric barriers, the small concentrations of the silica particles, and the close matching of the refractive indices of the solvent and polymer particles in these suspensions, that van der Waals attractions should be effectively eliminated. For a mixture such as this, consisting of dynamically identical but optically contrasting particles, the particle positions $\mathbf{r}_j$ and their scattering amplitudes $b_j(q)$ are statistically independent, so that the measured intermediate scattering function $F^{(m)}(q,\tau)$ is resolved as follows [25]:

$$F^{(m)}(q,\tau) = (N\overline{b^2})^{-1}\left\langle \sum_{j,k} b_j b_k \exp\{i\mathbf{q}\cdot[\mathbf{r}_j(0)-\mathbf{r}_k(\tau)]\}\right\rangle = \frac{\overline{b^2}}{\overline{\overline{b^2}}} F(q,\tau) + \left(1-\frac{\overline{b^2}}{\overline{\overline{b^2}}}\right) F_s(q,\tau), \quad (1)$$

where $\overline{b^m} = N^{-1}\Sigma_j b_j^m(q)$,

$$F(q,\tau) = N^{-1}\left\langle \sum_{j,k} \exp\{i\mathbf{q}\cdot[\mathbf{r}_j(0)-\mathbf{r}_k(\tau)]\}\right\rangle \quad (2)$$

is the coherent ISF,

$$F_s(q,\tau) = \langle \exp[i\mathbf{q}\cdot\Delta\mathbf{r}(\tau)]\rangle \quad (3)$$

is the self-ISF, and $\Delta\mathbf{r}(\tau)$ is a particle's displacement in time τ. Angular brackets appearing above denote ensemble averages. The zero-time values of the above ISF's are $F_s(q,0) = 1$ and $F(q,0) = S(q)$, where $S(q)$ is the static structure factor. After expanding the exponential in Eq. (1) and ensemble averaging individual terms, one arrives at the following result [26]:

$$F_s(q,\tau) = \exp\left[-\frac{q^2\langle\Delta r^2(\tau)\rangle}{6}\right] \times\left\{1+\frac{1}{2}\left[\frac{q^2\langle\Delta r^2(\tau)\rangle}{6}\right]^2\alpha_2(\tau)+\cdots\right\}, \quad (4)$$

where

$$\alpha_2(\tau) = \frac{3\langle\Delta r^4(\tau)\rangle}{5\langle\Delta r^2(\tau)\rangle^2} - 1 \quad (5)$$

is the first non-Gaussian correction to the distribution of particle displacements. Equation (4), truncated at the second term in the curly brackets, can be solved for $\langle\Delta r^2(\tau)\rangle$, the particle mean-squared displacement (MSD), and $\alpha_2(\tau)$ from measurements of $F_s(q,\tau)$ made at two different wave vectors. Alternatively, $\langle\Delta r^2(\tau)\rangle$ can be extracted from the Gaussian approximation for the self-ISF,

$$F_s(q,\tau) = \exp\left[-\frac{q^2\langle\Delta r^2(\tau)\rangle}{6}\right], \quad (6)$$

which is recovered from Eq. (4) when the quantity $q^2\langle\Delta r^2(\tau)\rangle/6$ is small. This result approximates in the time window where $F_s(q,\tau) > e^{-1}$, i.e., at short times or at small q, where $\ln[F_s(q,\tau)]/q^2 = -\langle\Delta r^2(\tau)\rangle/6$ is independent of q. Short- and long-time single-particle diffusion coefficients, D_s and D_l, are defined by

$$D_s = \lim_{\tau\to 0}\frac{\langle\Delta r^2(\tau)\rangle}{6\tau}, \quad D_l = \lim_{\tau\to\infty}\frac{\langle\Delta r^2(\tau)\rangle}{6\tau}. \quad (7)$$

At $\tau = 0$, Eq. (1) reduces to

$$F^{(m)}(q,0) = \frac{\overline{b^2}}{\overline{\overline{b^2}}} S(q) + \left(1-\frac{\overline{b^2}}{\overline{\overline{b^2}}}\right). \quad (8)$$

From Eq. (1) it follows that when the average scattering amplitude b vanishes, the only contribution to the measured ISF, $F^{(m)}(q,\tau)$, is the self-ISF. We determine this condition by varying the temperature of a crystallized suspension until the main Bragg reflection, centered at $q = q_m$ (where $q_m R \cong 3.4$), is no longer visible. The sample is rotated in the spectrometer during this process in order to optimize sampling over crystal orientations. By this means we find that $\overline{b}(q_m) = 0$ at the temperature $T_m = 20.4\,^\circ$C. Due to the presence of the stabilizing layer, the particles have a core-shell structure. Consequently, the match condition $\overline{b}(q) = 0$ is strictly obtained only at discrete wave vectors. However, we find that the initial decay of $F^{(m)}(q,\tau)$ scales with q^2, as expected for the self-ISF, over the range of wave vectors $0.3q_m \leqslant q \leqslant 1.3q_m$ at the temperature T_m. We infer, therefore, that scattering from the structure is suppressed, within experimental accuracy, not just at $q = q_m$ but over the whole

range of wave vectors where the measurements have been made. The latter ($0.3q_m \leqslant q \leqslant 1.3q_m$) corresponds to the range of spectrometer angles, $20° \leqslant \theta \leqslant 60°$, which is limited by the instrument at the lower end and an impracticably poor signal due to the emergence of multiple scattering (Sec. II C) at the other. Despite the fact that $b=0$, the amplitude of the incoherent ISF [the second term in Eq. (8)] is appreciable; inclusion of 2% silica particles increases the turbidity from 0.3 to 3.1 cm^{-1} at the match temperature. Hence the breakdown of the first Born approximation must be considered.

C. Dynamic light scattering: Suppression of multiple scattering

Dynamic light-scattering (DLS) measurements were performed with an ALV two-color multiple scattering suppression spectrometer, described in detail in Ref. [15]. In this instrument two focused laser beams, the blue (488 nm) and green (514 nm) lines of an argon ion laser, cross on the axis of the cylindrical sample cell. The main difference in our setup from that depicted in Ref. [15] is that the two colors are selected and separated by passing the beam of a single argon ion laser, operating simultaneously in all lines, through a triangular prism. Two detectors and associated detection optics are placed so that the detected beams have the same crossing angle as the incident beams. The relationship between this crossing angle and the scattering angle is such that the scattering process by the two colors incurs exactly the same momentum transfer (i.e., scattering vector **q**). Only the light that has been scattered once samples the same spatial Fourier component of the refractive index (or particle concentration) fluctuations for the two colors. Translational invariance in the sample ensures that only the singly scattered light survives cross correlation of the blue and green signals, I_B and I_G, from the two detectors. The resulting cross-correlation function,

$$g_c(q,\tau) = \frac{\langle I_B^s(q,0) I_G^s(q,\tau)\rangle}{\langle I_B^s(q)\rangle \langle I_G^s(q)\rangle}, \tag{9}$$

corresponds to the autocorrelation function $g(q,\tau)$ of a single spatial Fourier component of the intensity $I(q,\tau)$ of singly scattered light.

From the zero time value $g_c(q,0)$ of Eq. (9), one can calculate the ratio $\beta = \sqrt{\langle I_B^s\rangle\langle I_G^s\rangle}/\langle I_B\rangle\langle I_G\rangle$ of intensities corresponding to single and total scattering of light by the sample [15]. This quantity, shown in Fig. 1, illustrates the magnitude of multiple scattering typical in our samples. Figure 2 compares ISF's obtained from the standard autocorrelation function of the total scattered intensity, of either the blue or green laser lines, with that obtained from the cross-correlation function [Eq. (9)]. One sees that the distortion of the ISF's caused by multiple scattering, while negligible at the larger wave vector, is appreciable at the lower wave vector, particularly at intermediate and long times. On the other hand, it appears that for dilute suspensions, which have turbidity comparable to that of the concentrated sample studied here, multiple scattering distorts the ISF at short times (see Fig. 6 of Ref. [15]). These examples illustrate that the influence of multiple scattering is, in general, difficult to gauge. Although multiple scattering can, to an extent, be eliminated by using sample cells with shorter path lengths, their use severely impedes mixing of the most concentrated and viscous of the samples studied here.

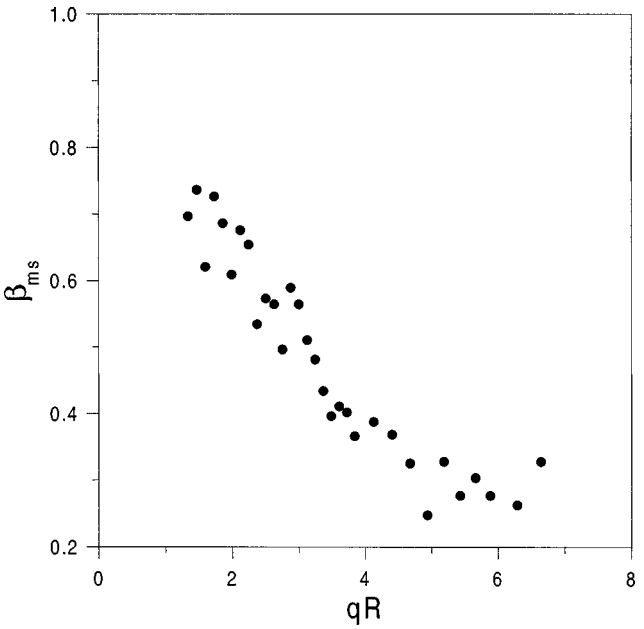

FIG. 1. The quantity β as a function of qR showing the magnitude of multiple scattering in a suspension at $\phi = 0.5$.

Even when the multiple scattering suppression instrument is optimally aligned, the overlap of scattering volumes corresponding to the two colors is still incomplete. This, plus the effects of multiple scattering, reduces the amplitude of the (normalized) intensity correlation function (ICF) [15]. Thus, even for a dilute (ergodic) sample, the zero time value $g(q,\tau)$ of the ICF measured by a cross-correlation, multiple scattering suppression instrument is less than the ideal value of 2 expected when the light scattered by the (Gaussian) temporal fluctuations of a single spatial Fourier component of the concentration is intercepted by one detector. It is not possible in practice to unambiguously resolve the effects on $g(q,0)$ due to incomplete overlap of scattering volumes, multiple scattering, and suppression of concentration fluctuations in a (nonergodic) sample. Consequently, the procedure introduced by Pusey and van Megen [27], which relates the (ensemble-averaged) ISF to a single measurement of the time-averaged ICF for a nonergodic sample, but which assumes that any reduction in $g(q,0)$ from an ideal value is entirely due to suppression of concentration fluctuations on the experimental time scale, can no longer be applied. For this reason, and also because we want to avoid any assumption concerning the duration of concentration fluctuations relative to the experimental time, we employ the more elaborate procedures for obtaining estimates of ensemble-averaged quantities discussed below.

D. Dynamic light scattering: Ensemble averaging

For sample volume fractions ϕ less than about 0.56, the slowest concentration fluctuations relax in less than about 10 s [4,5]. Therefore, an experiment lasting several thousand seconds captures a sufficiently large number of independent fluctuations that is representative of the ensemble. In these

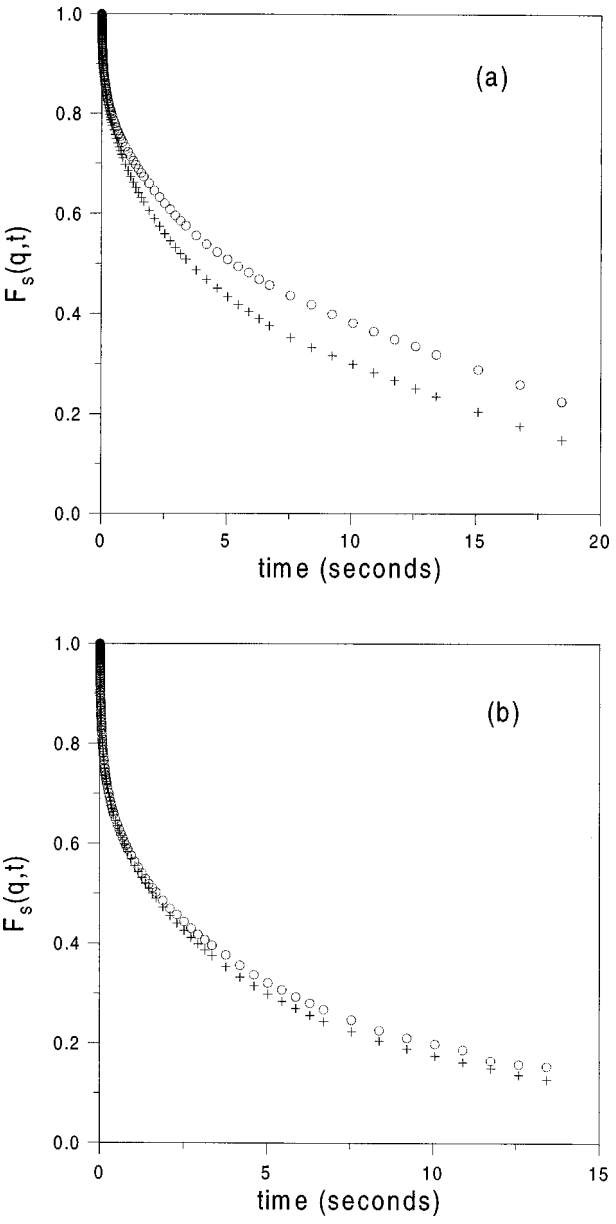

FIG. 2. Self-intermediate scattering functions obtained from the cross-correlation function (open circles) of the intensities I_B and I_G and the autocorrelation function (pluses) of either I_B or I_G in a suspension at $\phi=0.5$, as a function of time (in seconds): (a) $qR=2.9$ and (b) $qR=3.9$.

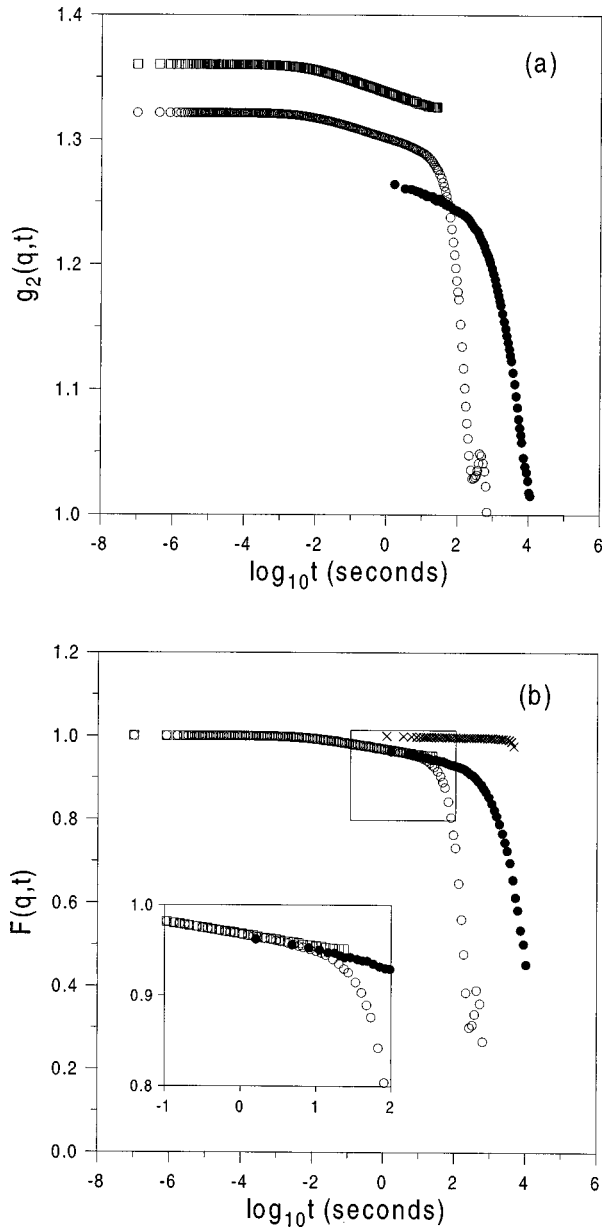

FIG. 3. Results, for $\phi=0.565$, obtained by continuous sampling (open circles), ''brute force'' method (open squares), interleaved sampling (closed circles), and quartz glass (crosses). (a) Normalized intensity autocorrelation functions and (b) intermediate scattering functions vs log time (seconds). Inset shows the time interval where continuous sampling and the ''brute force'' methods overlap.

cases the time-averaged ICF, measured in a DLS experiment, is equivalent to its ensemble average, i.e.,

$$g(q,\tau)=\frac{\langle I(q,0)I(q,\tau)\rangle_T}{\langle I(q)\rangle_T^2}=\frac{\langle I(q,0)I(q,\tau)\rangle_E}{\langle I(q)\rangle_E^2}. \quad (10)$$

Here $I(q,\tau)$ is the instantaneous intensity at time τ, q is the magnitude of the scattering vector, and $\langle\ \rangle_T$ and $\langle\ \rangle_E$ denote time and ensemble averages.

When the sample volume fraction is increased beyond about 0.56, fluctuation times lengthen to an extent where they approach and ultimately exceed the measurement time T ($\sim$10 000 s). In these cases we use a combination of two methods.

(i) The first, described by Xue *et al.* [28], entails continuous measurement of the ICF while the sample is rotated at a constant speed of about 10^{-4} revolutions per second. The resulting ICF, $g_c(q,\tau)$, has a cutoff at a time $\tau_c\sim 1$ s that corresponds to the residence time of a speckle at the detector. However, since the number of independent spatial Fourier components sampled in this process is of order 10^4, it is expected to yield a reasonable estimate of the ensemble average for the ICF for delay times up to τ_c.

(ii) The second method measures the ICF for longer delay times. The clock in a computer controls sample rotation, achieved by a stepper motor, and also sequentially triggers up to 4000 correlators in the computer software [29]. The rotational frequency $\sim 1\ \mathrm{s}^{-1}$ was chosen so that there is some

overlap of the delay times of the ICF, $g_I(q,\tau)$, obtained in this interleaved sampling scheme and that, $g_c(q,\tau)$, obtained by continuous sampling. In order to avoid the possibility of shearing the sample in the scattering volume, centered on the cell axis, the sample cell was slowly accelerated to a constant rotational frequency. About 30 min were then allowed to elapse before commencing the measurement. No influence on the measured correlation functions was observed when these startup conditions were varied.

Clearly, the efficacy of this method relies on the ability of the mechanism to return the same speckle(s) to the detector for each revolution. Reduction in amplitude of the ICF, amounting to 40%, due to the combined effects of random repositioning errors and averaging over multiple speckles, was determined by measuring $g_I(q,\tau)$ of a cylindrical quartz rod. However, since no appreciable decay of the ISF is evident at long times [Fig. 3(b)], systematic repositioning errors or long-term instabilities in the equipment are negligible. Differences of the amplitudes of the ICF's obtained by the two methods necessitates scaling of $g_I(q,\tau)$ so that it meshes with $g_c(q,\tau)$ around τ_c.

The ICF obtained by combining these procedures is regarded as the ensemble-averaged ICF, $g(q,\tau)$ defined in Eq. (10), and, like the result obtained by the more straightforward standard method for less concentrated suspensions, is related to the ISF, $F^{(m)}(q,\tau)$, by the usual Siegert relationship [30],

$$g(q,\tau)=1+c\left|\frac{F^{(m)}(q,\tau)}{F^{(m)}(q,0)}\right|^2. \tag{11}$$

The quantity $c(\leqslant 1)$ is determined by the random repositioning errors, mentioned above, by the ratio of the coherence area, or speckle size, to the detector area, and by the factors associated with suppression of multiple scattering discussed in Sec. II C.

ICF's obtained by the methods described above are shown in Fig. 3(a). Also shown is the ICF obtained by a ''brute force'' (ensemble) average (described in Ref. [4]) over 4000 independent measurements of 75 s duration. The ISF obtained from these data after scaling is shown in Fig. 3(b). Note that up to the cutoff time, $\tau_c \sim 1$ s, the ISF's determined by continuous sampling and the ''brute force'' method are indistinguishable. Significantly, the final ISF represents an average over several thousand independent spatial Fourier components of the sample's refractive index fluctuations and spans a time window of more than 11 decades.

III. RESULTS AND DISCUSSION

A. Self-intermediate scattering functions: Non-Gaussian effects

In the following, all distances are expressed in units of the particle radius, R, and times in units of the Brownian time, $\tau_b=R^2/(6D_0)$ $(=0.0215\ \mathrm{s})$, where D_0 is the free-particle diffusion constant. In these units, $\langle \Delta r^2(1)\rangle=1$ for a freely diffusing particle.

Figure 4 shows self-ISF's for $\phi=0.405$, expressed as $-6(qR)^{-2}\ln F_s(q,\tau)$ versus τ, for several wave vectors. Mean-squared displacements obtained from these results are also shown. At short times [Fig. 4(a)] the data converge to a single curve indicating that scattering from the structure (i.e., the coherent ISF) has been suppressed. In view of this, the systematic departures from q^2 scaling seen at longer times [Fig. 4(b)] must, according to Eq. (4), be due to non-Gaussian effects. The double logarithmic plot [Fig. 4(c)] presents a better display of the dynamic range.

As in earlier work [24], we also find here in the case of the equilibrium fluid ($\phi<\phi_f$) that the maximum value, $\alpha_{\max}[=\max(\alpha_2(\tau))]$, of the non-Gaussian term compatible with these data is no more than about 0.2. Such small non-Gaussian effects will be hidden by random experimental errors unless the ISF's are based on exceedingly large ensembles of independent fluctuations [31]. At much higher volume fractions, such as $\phi=0.583$ also shown in Fig. 4, deviations from q^2 scaling are random, despite the fact that each of the ISF's comprises an average over some 4000 independent spatial Fourier components of the concentration fluctuations. A consequence is that, within experimental noise, the quantity $(-6/q^2)\ln(F_s(q,\tau))$ is independent of wave vector [Fig. 4(c)]. So for the purpose of discussing the large changes in particle dynamics that accompany traversal of the GT (Sec. III C), we presume that a good estimate of the MSD can be obtained by invoking the Gaussian approximation [Eq. (6)] for the self-ISF measured at $q=0.3q_m$ $(qR=1.3)$.

In an attempt to quantify the maximum possible value of the non-Gaussian term that could be hidden by the noise in the data, we calculate $F_s(q,\tau)$ from Eq. (4), truncated at the second term in the curly brackets, for several wave vectors, $1\leqslant qR\leqslant 5$, spanned in our experiments. For this purpose we employ the following expressions for the MSD [32] and $\alpha_2(\tau)$ [33]:

$$\langle \Delta r^2(\tau)\rangle=\tau-(1-D_l)(\tau+e^{-\tau}-1), \tag{12}$$

$$\alpha_2(\tau)=\frac{\alpha_{\max}\tau}{(\tau+1)^2}. \tag{13}$$

We note that the ISF calculated from the above expressions does not describe all of the features, such as stretching, observed in relaxation functions in the vicinity of the GT. However, they suffice for the present purpose, which is to determine the extent to which non-Gaussian contributions to the particle displacements cause deviations from q^2 scaling of the self-ISF's. In Eqs. (12) and (13), the time $\tau=1$ represents the beginning of the crossover from small-scale to large-scale diffusion and D_l is the long-time self-diffusion coefficient as defined in Eq. (7). Equation (12) is a result of the trapping diffusion model, proposed by Hiwatari *et al.* [33], and it is selected here simply because it ensures that the non-Gaussian term is small at short times, increases to $\alpha_{\max}$ at $\tau=1$, and converges to zero at long times. Results for $\log_{10}[(-6/q^2)\ln(F_s(q,\tau))]$ computed with Eqs. (12), (13), and (4) are shown in Fig. 5 for two values of D_l and two values for $\alpha_{\max}$. Note that the respective axes of the computed (Fig. 5) and experimental [Fig. 4(c)] results span the same ranges. For the reason mentioned above, the precise extent of compatibility of the computed and experimental results is not important *per se*. However, a comparison at

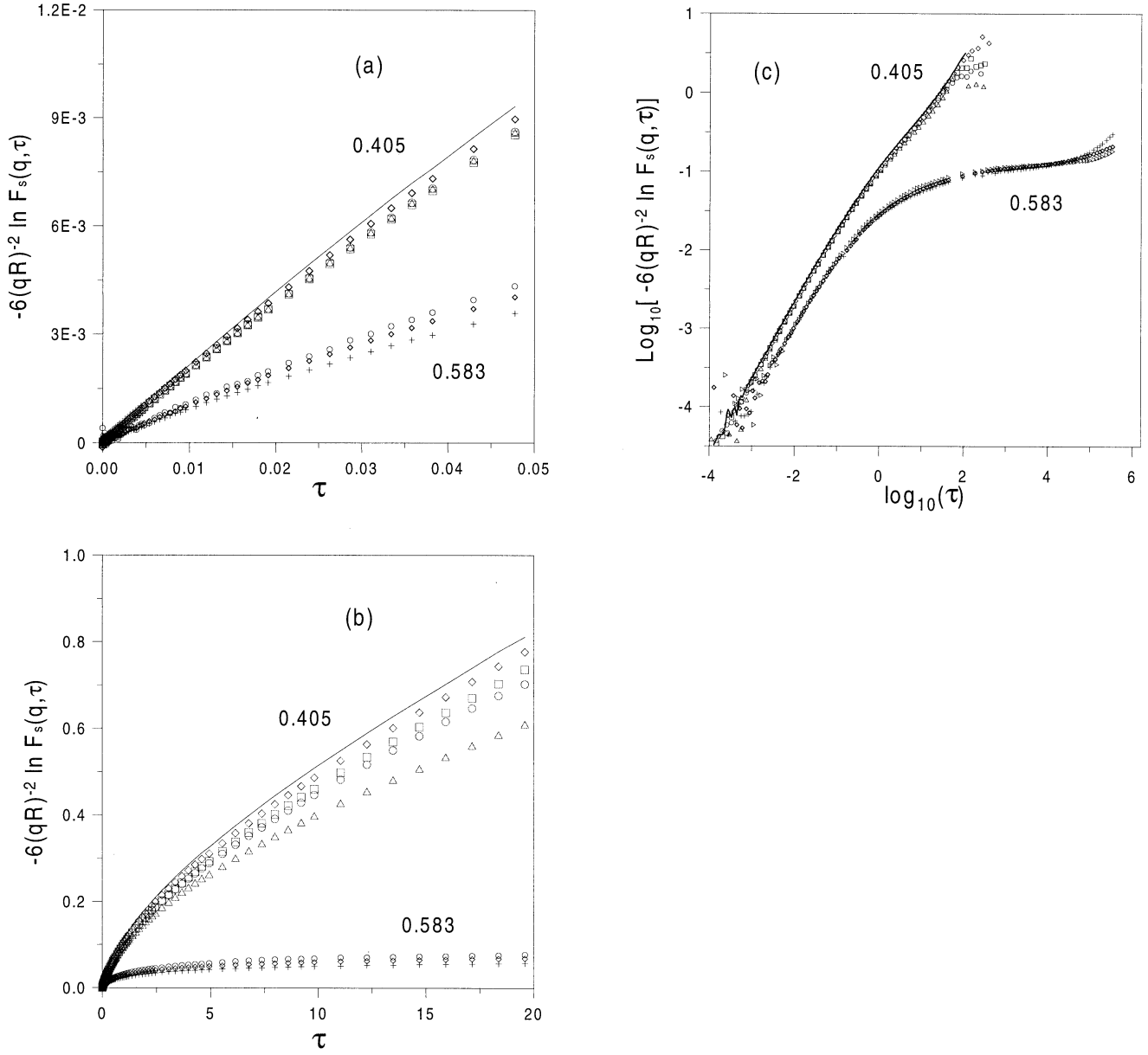

FIG. 4. Particle mean-squared displacements (solid line) and the quantity $-6(qR)^{-2}\ \ln F_s(q,\tau)$ at $qR=2.0$ (diamonds), 2.9 (squares), 3.4 (circles), and 3.8 (triangles) as functions of (dimensionless) time for $\phi=0.405$, and $qR=1.3$ (pluses), 3.8 (diamonds), and 5.3 (circles) for $\phi=0.583$. (a) and (b) display the results on different time scales. (c) The particle mean-squared displacement and the quantity $\log_{10}[-6(qR)^{-2}\ \ln F_s(q,\tau)]$ vs the logarithm of (dimensionless) time. Note that in this and the following figures, time is expressed in units of the Brownian time, $\tau_b=R^2/(6D_0)$.

both volume fractions does reveal that the largest systematic deviations from q^2 scaling in $F_s(q,\tau)$ that could possibly be obscured by the noise in the data may correspond to a non-Gaussian contribution no larger than about 0.2. Similar results are obtained for volume fractions between those depicted in Fig. 4.

We will show below (Sec. III B) that the suspension undergoes a GT at $\phi_g=0.573$. Hence, the more interesting import of the above results is that there is no noticeable increase in non-Gaussian effects as the GT is traversed from the fluid side. We point out, however, that this inference applies to times for which the MSD $\langle\Delta r^2(\tau)\rangle\lesssim 1$ in the fluid or, in the case of the glass, $\langle\Delta r^2(\tau)\rangle\lesssim 0.1$. Beyond this our data, mainly for larger values of the wave vector, become increasingly subject to statistical errors [bear in mind that $F(q,\tau)\sim\exp(-q^2D\tau)$]. As discussed in Ref. [24], in order to be confident that the ISF's are not affected by systematic errors incurred by scattering from the structure, it is advisable to base the calculation of $\alpha_2(\tau)$ on self-ISF's measured over a range of wave vectors that span the position of the first maximum of the structure factor.

Computer simulations, both molecular [33,34] and Brownian [35] dynamics, find that correlated jump motions become increasingly prevalent as a liquid is supercooled. Moreover, these atoms, with appreciably larger than average mobility, occur in clusters whose size increases with (super)cooling [36]. However, their occurrence, manifested macroscopically by non-Gaussian displacement statistics, is

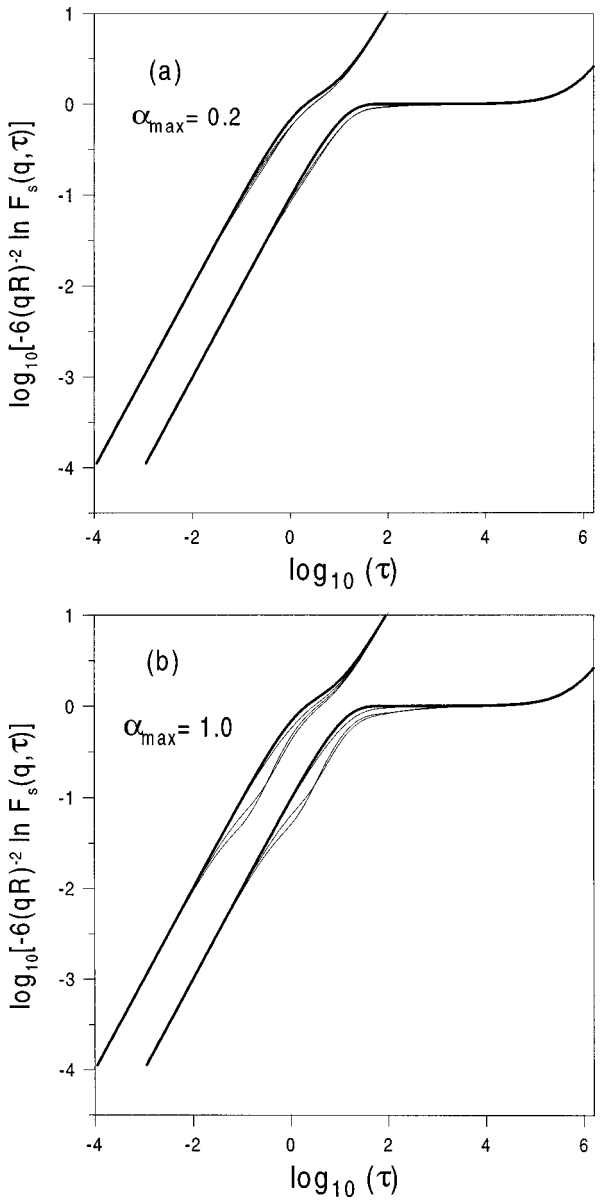

FIG. 5. The quantity $\log_{10}[-6(qR)^{-2} \ln F_s(q,\tau)]$ calculated from Eqs. (12), (13), and (4) for $\log_{10}(D_l) = -1$ (upper curves) and -5 (lower curves) for $qR = 1$, 3, and 5 shown as functions of the logarithm of time. The bold curves show $\log_{10}[\langle \Delta r^2(\tau) \rangle]$.

not evident until the average atomic motion, as read from the MSD, has become diffusive, i.e., where $\langle \Delta r^2(\tau) \rangle \approx 1$ [37]. Thus, on the basis of the present results the behavior of colloidal suspensions should not necessarily be seen as contradictory to that found in computer simulations of atomic fluids. We are investigating this issue further and we anticipate reporting on it in the near future.

B. Self-intermediate scattering functions: Mean-squared displacements

Figure 6 shows the self-ISF's, measured at $qR = 1.3$, versus dimensionless time for volume fractions ranging from infinite dilution to $\phi = 0.583$. Note the progressively slower decay of the ISF's as the suspension's volume fraction is increased. The sample at $\phi = 0.566$ is the most concentrated for which the ISF still decays to zero in the experimental time of $\tau = 10^6$ (this corresponds to about 2×10^4 s). The ISF's of suspensions at higher volume fractions fail to decay completely in the experimental time window although they show some downward curvature at long times. We will discuss this feature in Sec. III C.

As discussed in Sec. III A, the quantities $\log_{10}[(-6/q^2)\ln(F_s(q,\tau))]$ measured at $qR = 1.3$ are now equated with the MSD's [Eq. (6)] and are presented in the form of double-logarithmic plots as functions of time in Fig. 7. Diffusive motion [i.e., where $\langle \Delta r^2(\tau) \rangle \propto \tau$] can be identified by those regions where the data follow straight lines of unit slope. As expected, this occurs over the whole range of accessible times only for a very dilute suspension, where the particle motion is characterized by the free-particle diffusion coefficient D_0. At higher volume fractions, diffusive motion is seen at short times, prior to appreciable change to the particle MSD [$\langle \Delta r^2(\tau) \rangle \lesssim 0.01$], and at long times [$\langle \Delta r^2(\tau) \rangle \gtrsim 1$] during which a particle experiences many (statistically independent) environments of neighbors. The increasing persistence of this environment, expected with increasing volume fraction, is indicated in the lengthening subdiffusive region that connects the short- and long-time diffusive motions. For $\phi > 0.573$ it is no longer possible to unambiguously identify a diffusive regime at long times.

Short- and long-time self-diffusion coefficients, D_s and D_l, are shown in Fig. 8 along with corresponding results of earlier measurements from Ref. [16]. Where the two sets of results overlap, $0.4 < \phi < 0.5$, discrepancies are apparent. We proffer two possible sources of overestimation of the long-time diffusion coefficients in Ref. [16]. First, in the older work the effects of multiple scattering were not considered. One sees from Fig. 2 that multiple scattering enhances the rate of decay of the ISF's. Second, the linear, 100-channel, single-bit correlator used in the experiments of Ref. [16] limits more severely than that of the ALV5000 correlator used here, the extent to which the decay of ICF's can be followed to long times.

The ratio D_l/D_s represents a quantitative indication of the lengthening, or ''stretching,'' of self-ISF's as ϕ is increased. One can readily verify that at infinite dilution $D_l/D_s = 1$, whereas at $\phi = 0.566$ $D_l/D_s \approx 4 \times 10^{-5}$. These results also suggest the convergence of D_l to zero, i.e., a glass transition, at $\phi_g = 0.57$. However, small-scale motion, indicated by D_s, persists beyond this volume fraction and it is not until the particles are fully compressed, by centrifuging the suspension to random close packing, that no decay of the ISF is observed (see Fig. 5 of Ref. [38]). In the absence of solvent-mediated hydrodynamic interactions $D_s = D_0$ [10], i.e., the short-time diffusion coefficient is independent of the volume fraction. Thus the reduction in D_s seen with increasing ϕ, and its possible convergence to zero at ϕ_r, must be due entirely to hydrodynamic effects.

C. The glass transition

The suggestion of a GT at $\phi_g = 0.57$ seems incompatible with the persistent downward curvature of the self-ISF's at long times (Fig. 6), even when the suspension volume fraction is increased beyond 0.57. Note that, due to the slightly larger polydispersity and the more efficient procedures for estimating ensemble averages, it has been possible to extend

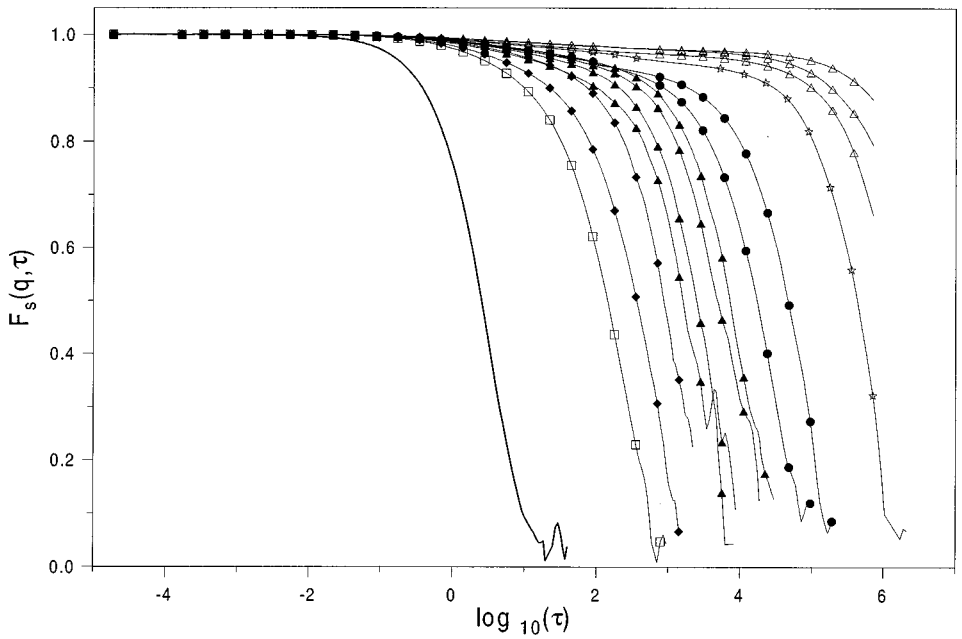

FIG. 6. Self-intermediate scattering functions, $F_s(q,\tau)$, vs logarithm of (dimensionless) time for suspension volume fractions (left to right) $\phi \approx 0$ (bold line), 0.466 (squares), 0.502, 0.519 (closed diamonds), 0.534, 0.538, 0.543, 0.548 (closed triangles), 0.553, 0.558 (closed circles), 0.566 (stars), and 0.573, 0.578, 0.583 (open triangles).

the experimental time window by about one decade beyond that attained in previous work [4,5] in which these slow decays were not detected. Similar slow decays have been observed in ''glasses'' of suspensions of cross-linked microgels [39]. Nonetheless, the mere escape of the slowest relaxation processes from the experimental window might not in itself be considered adequate evidence for a glass transition.

To illustrate the change in the nature of the decay when the volume fraction of the suspension approaches and then exceeds 0.573, we show in Fig. 9 ISF's for $\phi = 0.566$ and 0.583 at different waiting times, τ_w. The waiting time is the time the suspension is left undisturbed after tumbling before commencement of the DLS measurement. For the higher volume fraction the downward curvature of the ISF's extends to longer times as τ_w is increased. For $\phi = 0.566$ the ISF's coincide once a certain waiting time is exceeded. We should also point out that after thermal equilibration (about 15 min) of the suspensions in the spectrometer, ISF's measured at lower volume fractions ($\phi \leqslant 0.558$) are independent of the waiting time.

We rationalize these observations as follows. Immediately following the quench, effected here by tumbling, a suspen-

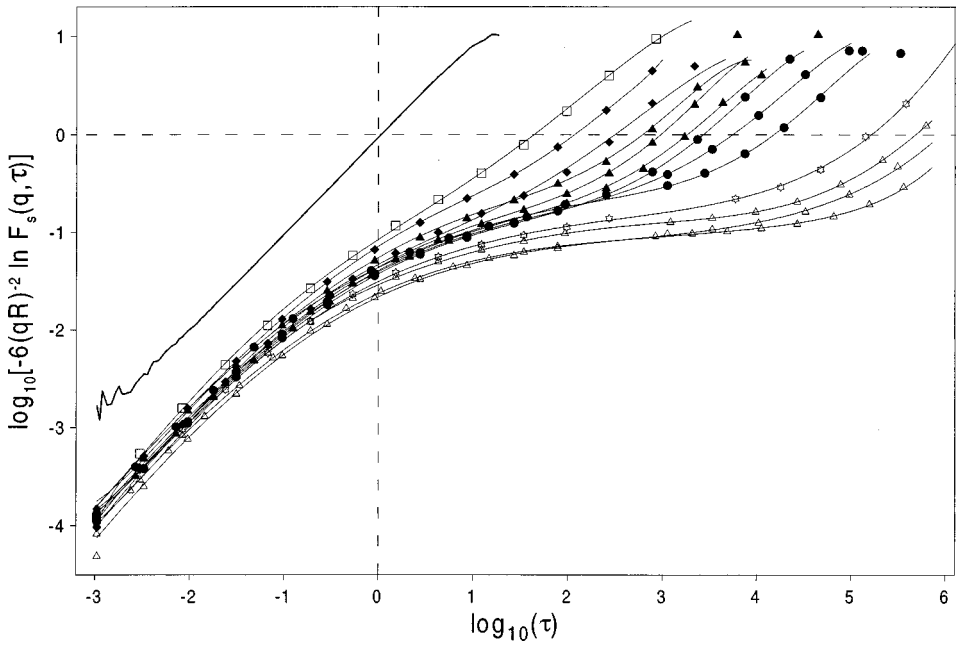

FIG. 7. Logarithm of the particle mean-squared displacements vs logarithm of (dimensionless) time, for volume fractions increasing from left to right as indicated in Fig. 6.

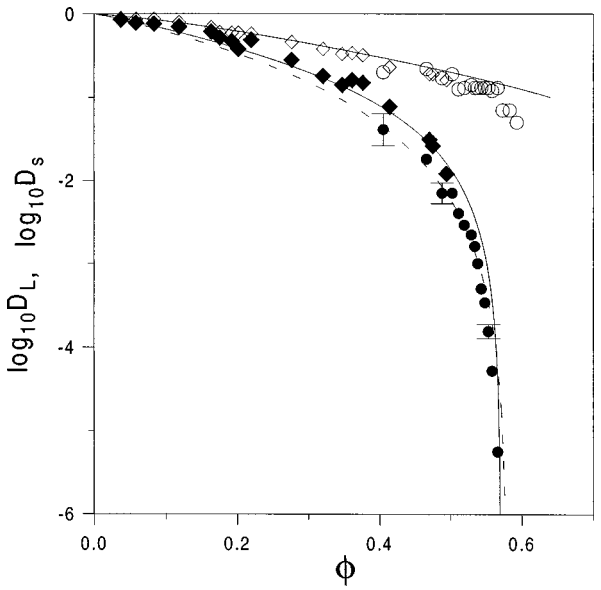

FIG. 8. Short- (open symbols) and long- (closed symbols) time diffusion coefficients, defined in Eq. (7), vs volume fraction. Diamonds are the data from Ref. [16] and circles are the results from this work. The upper and lower solid curves, respectively, represent the predictions for D_s and D_l from Ref. [44], and the dashed curve is the function $(1-\phi/\phi_g)^{2.6}$, predicted by MCT, with $\phi_g=0.57$.

sion is in a state of nonequilibrium from which equilibrium may or may not be attained. The polydispersity of the suspensions, with the attendant high nucleation barrier relative to that of a one-component system, ensures that the ensuing relaxation processes are unlikely to be influenced by nucleation. Should the quenched nonequilibrium fluid relax to a state of (metastable) equilibrium, then it would seem plausible that it does so by the same diffusive processes, and therefore on the same time scale τ_r, as structural relaxation measured by the ISF's. For $\phi\leqslant 0.558$, relaxation times are short compared with the experimental time, and the fact that the measured ISF's are independent of τ_w indicates that these pertain to fluids in states of (metastable) equilibrium. By the same token, the waiting time dependence of the ISF's of suspensions at the higher volume fractions in excess of $\phi_g=0.57$ suggests these remain in states of nonequilibrium. In fact, they do so for many weeks, before settling of the particles becomes appreciable. The sample at $\phi=0.566$ lies at the crossroads. For this case the relaxation time is comparable with the measurement time, but once this is exceeded, i.e., $\tau_w>\tau_r$, the fluid has attained (metastable) equilibrium since from then on the measured ISF's are independent of the waiting time. Accordingly we identify ϕ_g as the volume fraction of the ergodic to nonergodic (or glass) transition, the volume fraction where the colloidal fluid falls out of equilibrium.

D. Comparison with theory

Cummins *et al.* have recently presented a fairly exhaustive classification and critical review of the theories that describe dynamical properties of materials in the vicinity of the GT [40]. Among these, mode-coupling theory (MCT) stands out as the most detailed in terms of predictions; when the idealized version of MCT is applied to the hard-sphere system, all parameters, save an overall scaling time, required to specify the relaxation functions are given [41].

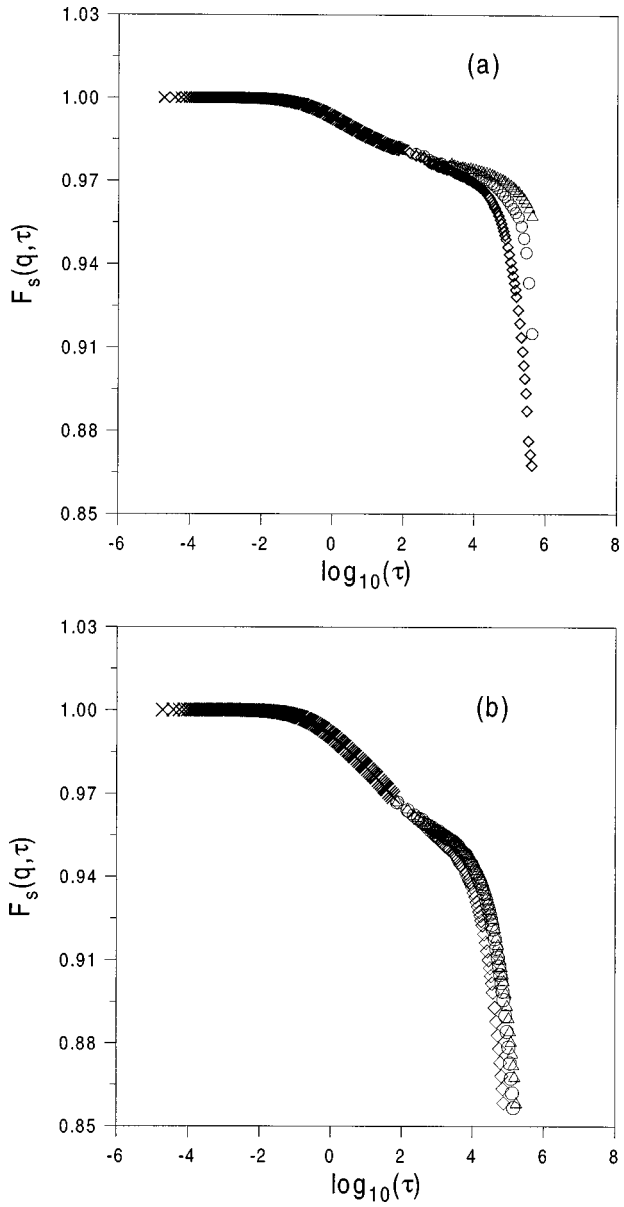

FIG. 9. Self-intermediate scattering functions vs logarithm of (dimensionless) time for (a) $\phi=0.583$ for waiting times τ_w given by $\log_{10}(\tau_w)=5.2$ (diamonds), 6.7 (circles), 7.5 (triangles) and (b) $\phi=0.566$ for $\log_{10}(\tau_w)=5.3$ (diamonds), 6.6 (circles), 7.1 (triangles).

An alternative theory developed specifically to describe the GT in colloidal suspensions of hard spheres was recently proposed by Tokuyama *et al.* [42]. This theory calculates the self-ISF from a linear diffusion equation while the system progresses from an initial nonequilibrium state to equilibrium. It follows that once equilibrium is attained, the ISF becomes a single exponential in time. We face two difficulties when attempting to discuss our results in terms of this theory. The first is that the ISF's deviate appreciably from a single exponential under conditions in which the samples are, as far as we can ascertain experimentally, in states of (metastable) equilibrium. The second is that, while one could possibly explore the dissipation of the initial nonequilibrium quenched state very close to the GT ($\phi\lesssim\phi_g$), we see no

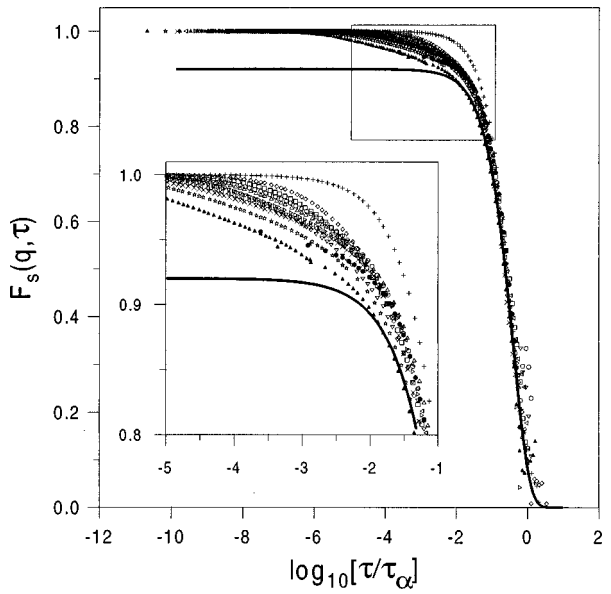

FIG. 10. Self-intermediate scattering functions as functions of the logarithm of the rescaled time, τ/τ_α. The solid curve represents the function, $f_c \exp[-(\tau/\tau_\alpha)^\beta]$, with $f_c=0.93$ and $\beta=0.95$.

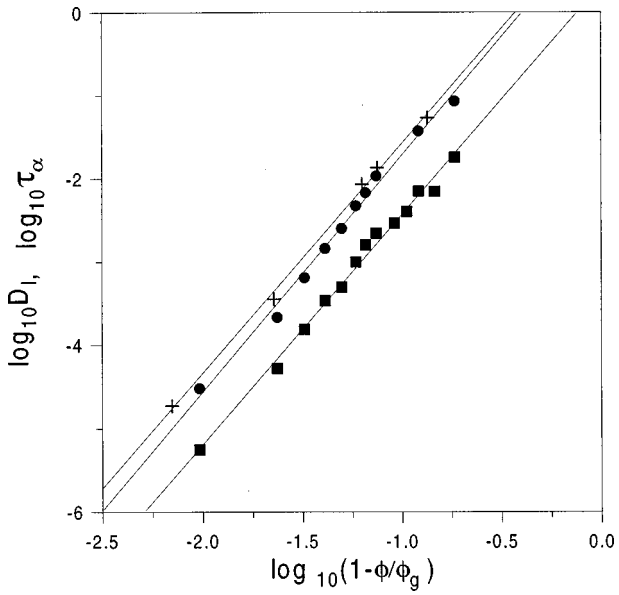

FIG. 11. Logarithms of the (long-time) self-diffusion coefficients, D_l (squares), and the relaxation rates, τ_α^{-1} (circles), vs the quantity $(1-\phi/\phi_g)$. The pluses indicate relaxation rates obtained from the coherent intermediate scattering functions in Ref. [4]. See text for further details.

experimental means at present to unambiguously determine the initial nonequilibrium condition, the volume fraction distribution $\phi(\mathbf{r})$, required by the theory.

MCT, on the other hand, describes relaxation of the ISF's by means of a nonlinear equation for systems in equilibrium. Therefore, this theory is predicated on conditions that correspond to those of the above experiments and it seems appropriate to discuss our results in terms of MCT.

Scaling of the data in time for $\phi \leqslant 0.566$ so that they coincide at long times (Fig. 10) illustrates time-density superposition and indicates that about 90% of the relaxation is due to the primary α process. The time-scaled ISF's coincide at long times with the stretched exponential function, $f_c(q)\exp[-(\tau/\tau_e)^\beta]$ with $f_c(q)=0.93\pm0.01$ and $\beta=0.95\pm0.02$. MCT predicts that the nonergodicity parameter, the amplitude of the α process, for the self-ISF at the wave vector, given by $qR=1.3$, is $f_c(q)=0.95$ [13,41]. The initial 10% of the relaxation is due to the small-scale diffusive motions and, in the terminology of MCT, the β process. The q^2 scaling of $\ln F_s(q,\tau)$, shown in Sec. III A, is also consistent with the idealized version of MCT [43].

In Fig. 8 one sees that the long-time diffusion coefficients are compatible with the power law $D_l \sim (1-\phi/\phi_g)^\gamma$ with $\gamma=2.6$ predicted by MCT [13]. Here we use the experimental value for the GT volume fraction $\phi_g=0.57$. Small-scale (microscopic) details have not been taken into account in MCT so far and, thus, this theory makes no prediction for the short-time diffusion coefficient, D_s. The theory of Tokuyama and Oppenhein [44], on the other hand, purports to account for the hydrodynamic interactions among colloidal hard spheres and, as seen in Fig. 8, the predictions of this theory for both D_s and D_l are compatible with the data up to about ϕ_g. However, given the noise in the experimental estimates of D_l and the fact that they decrease sharply as the GT is approached, the comparisons displayed in Fig. 8 do not present very sensitive tests of the theoretical predictions. In an alternative approach, bearing in mind that asymptotically close to the GT a power law $D_l \sim (1-\phi/\phi_g)^\gamma$ is predicted by both MCT ($\gamma=2.6$) and the theory of Tokuyama and Oppenheim ($\gamma=2$) for the long-time diffusion coefficient, we determine the optimum linear fit of $\log_{10} D_l$ versus $\log_{10}(1-\phi/\phi_g)^\gamma$ while treating ϕ_g and γ as free parameters. The result of this analysis, shown in Fig. 11, gives $\phi_g=0.571\pm0.001$ and $\gamma=2.7\pm0.1$. Interestingly, a similar result, $\phi_g=0.572\pm0.001$ and $\gamma=2.9\pm0.1$, is obtained when applying this analysis to the inverse of the scaling times, τ_α, required to cause the ISF's in Fig. 6 to coincide at long times as shown in Fig. 11.

In Ref. [4] it is shown that the coherent ISF's also satisfy this time-density superposition principle and that the corresponding scaling times, τ'_α, are independent of the wave vector. Application of the above fitting procedure to $(\tau'_\alpha)^{-1}$, also shown in Fig. 11, gives $\phi_g=0.572\pm0.001$ and $\gamma=2.8\pm0.2$. Figure 11 therefore indicates that when the relaxation rates of the α process, determined from either the coherent or self-ISF's, and the long-time self-diffusion coefficients are forced to a power-law dependence on the quantity $(1-\phi/\phi_g)$, the values of ϕ_g obtained agree with that where the ergodic to nonergodic transition is observed and the exponents obtained are consistent with the value $\gamma=2.6$ predicted by MCT [13]. The theory of Oppenheim and Tokuyama [44], on the other hand, constructed specifically for hard-sphere suspensions, predicts an exponent $\gamma=2$. The equality of power-law exponents associated with relaxation rates and diffusion coefficients, as predicted by MCT and confirmed here, is not supported by computer simulations of binary mixtures with Lennard-Jones interactions [45].

E. Crystallization and the glass transition

When our measurements are augmented by results of recent computer simulations, we see behavior, although in greater microscopic detail, similar to crystallization and glass

formation in metals and metal alloys. The latter behavior is usually discussed in terms of classical nucleation and growth models [46] and we shall attempt likewise. For this purpose we use the most rudimentary expression for the nucleation rate,

$$R \sim \tau_n^{-1} \exp(-\Delta G^*), \tag{14}$$

where $\Delta G^* (\sim \eta^3/\Delta\mu^2)$ is the nucleation barrier relative to the mean thermal energy, η is the surface tension of the crystal-fluid interface, and $\Delta\mu$ is the difference between the chemical potentials of the crystal and fluid. It has been demonstrated elsewhere [4,5] that homogeneous nucleation demands large-scale particle diffusion. Accordingly we assume $D_l \sim \tau_n^{-1}$. A fluid is unstable to nucleation, i.e., $\Delta G^* < 1$, once a certain degree of undercooling is exceeded. (Applying available computer simulation data for the surface tension and chemical potentials of crystal and fluid phases, one obtains for hard spheres, for example, $\Delta G^* < 1$ when $\phi \gtrsim 0.56$ [47].) Once nucleated crystal growth proceeds without thermodynamic resistance according to the Wilson-Frenkel law [12],

$$G \sim \tau_g^{-1} [1 - \exp(\Delta\mu)], \tag{15}$$

at speeds τ_g^{-1} proportional to the mean thermal velocity in atomic systems [46,48] and proportional to the short-time diffusion coefficient, D_S [Eq. (7)], in the case of colloidal systems [49]. Quenching a fluid to a point where large-scale diffusion is arrested is therefore not necessarily sufficient to produce an experimentally viable glass. Macroscopic impurities or nonequilibrium structures, necessarily induced when quenching through the range of temperatures or densities where the fluid is unstable to nucleation, may seed crystal growth.

Addition of (microscopic) impurities, in the case of metals [46], for example, or broadening the PSD, in the case of colloids [6], improves the glass-forming tendency for two reasons. First, inclusion of small amounts of a second component slows nucleation without appreciable influence on the long-time particle dynamics [14], i.e., the relaxation time appearing in Eq. (14). Therefore, the formation of critically sized nuclei requires motions on a scale comparable to the interparticle spacing irrespective of whether one is dealing with a one- or multicomponent fluid. If, as is the case in a eutectic forming mixture, partitioning of species is required on solidification, then, to a first approximation, this requirement enters Eq. (14) through an increase in ΔG^*. Second, the limiting growth velocity, τ_g^{-1}, is likely to be determined by the large-scale diffusion coefficient, D_l, rather than the small-scale diffusion coefficient, D_s, once an appreciable fraction, possibly of order 10%, of particles is required to be partitioned on solidification.

IV. CONCLUSIONS

We have presented measurements of self-intermediate scattering functions for suspensions, with hard-sphere-like interactions, in shear-melted amorphous states. The slowing down of particle diffusion observed with increasing volume fraction and its arrest at $\phi_g = 0.57$ are consistent with the behavior deduced from earlier measurements of coherent intermediate scattering functions on similar suspensions.

The nucleation barrier and kinetic resistance to crystal growth have been increased, although not entirely by design, by increasing the width of the PSD sufficiently to obtain experimentally viable metastable fluids and glasses without actually suppressing crystallization completely under all conditions. In turn, this has permitted measurements of the ISF's extending to longer delay times than previously, without concern for the possible effects of crystallization, and has exposed very slow, waiting-time-dependent decays in the glass phase, $\phi > \phi_g = 0.57$.

Work prior to that of this paper showed that provided the PSD is sufficiently narrow and shaped, so that fractionation of the components required for crystal formation [9,50] is not too great, crystal growth, significant in extent but slow in time, still occurs on nonequilibrium structures induced by the shear-melting process. It seems that in these cases crystal growth requires motions that are small compared with the interparticle spacing and the quenched-in structures provide the seeds by which the nonequilibrium glass channels its way to the stable equilibrium crystal. In the present work these channels are effectively closed by further broadening of the PSD.

We close with the conjecture that a hypothetical suspension of perfectly identical (hard) spheres is fundamentally no different from a one-component atomic system in that the glass of either, while having large-scale diffusion arrested, is unstable to crystal growth. Such growth may proceed at a rate proportional to the (root-mean-squared) thermal velocity in the case of an atomic system or the local (short-time) diffusion coefficient in a colloidal suspension. As indicated in Sec. III B, the latter motion still persists in the glass. Thermal or shear quenching through the range of temperatures or densities where the liquid is unstable to nucleation will necessarily produce nonequilibrium structures in the glass, some of which may seed crystal growth. It seems that increasing the quench rate only serves to increase the probability of inducing suitably structured and positioned seeds [51].

ACKNOWLEDGMENTS

We are grateful to Sylvia Underwood for preparation of the colloidal particles used in this work, to Phil Francis for technical assistance, and the Australian Research Council for financial support. We also acknowledge fruitful discussions with Bruce Ackerson, Wolfgang Götze, Peter Harrowell, Peter Pusey, Ian Snook, and Michio Tokuyama.

[1] M. D. Rintoul and S. Torquato, Phys. Rev. Lett. **77**, 4198 (1996).
[2] L. V. Woodcock, Ann. (N.Y.) Acad. Sci. **37**, 274 (1981).
[3] J. Jäckle, Rep. Prog. Phys. **49**, 171 (1986).
[4] W. van Megen and S. M. Underwood, Phys. Rev. E **49**, 4206 (1994).
[5] W. van Megen, Transp. Theory Stat. Phys. **24**, 1017 (1995).
[6] S. I. Henderson, T. C. Mortensen, S. M. Underwood, and W.

van Megen, Physica A **233**, 102 (1996).
[7] W. B. Russel, P. M. Chaikin, J. Zhu, W. V. Meyer, and R. Rogers, Langmuir **13**, 3871 (1997).
[8] P. N. Pusey and W. van Megen, Nature (London) **320**, 340 (1986).
[9] W. van Megen and S. M. Underwood, Nature (London) **362**, 616 (1993).
[10] P. N. Pusey, in *Liquids, Freezing and the Glass Transition*, edited by J. P. Hansen, D. Levesque, and J. Zinn-Justin (North-Holland, Amsterdam, 1991), p. 763.
[11] P. M. Chaikin, J. M. di Meglio, W. D. Dozier, and H. M. Linday, in *Physics of Complex and Supermolecular Fluids*, edited by S. A. Safran and N. A. Clark (Wiley, New York, 1987).
[12] J. Frenkel, *Kinetic Theory of Liquids* (Oxford University Press, Oxford, 1946).
[13] W. Götze, in *Liquids, Freezing and the Glass Transition*, edited by J. P. Hansen, D. Levesque, and J. Zinn-Justin (North-Holland, Amsterdam, 1991), p. 287; W. Götze and L. Sjögren, Rep. Prog. Phys. **55**, 241 (1992).
[14] S. I. Henderson and W. van Megen, Phys. Rev. Lett. **80**, 877 (1998).
[15] P. N. Segrè, W. van Megen, P. N. Pusey, K. Schätzel, and W. Peters, J. Mod. Opt. **42**, 1929 (1995).
[16] W. van Megen and S. M. Underwood, J. Chem. Phys. **91**, 552 (1989).
[17] S. M. Underwood and W. van Megen, Colloid Polym. Sci. **274**, 1072 (1996).
[18] P. N. Pusey and W. van Megen, J. Chem. Phys. **80**, 3513 (1984).
[19] The apparent wave-vector-dependent diffusion coefficients, $D(q)$, shown in Refs. [15] and [18] for dilute suspensions of PMMA particles, show symmetrical deviations about $D(q \rightarrow 0)$. These results were interpreted in terms of symmetrical PSD's. For the *p*-(TFEA/MMA) particles used here these deviations are asymmetrically biased toward smaller values. For a given PSD, $D(q)$ and the intensity $I(q)$ are readily evaluated numerically [18]. The asymmetrical PSD discussed in the text reproduces both the measured $D(q)$ and intensities $I(q)$.
[20] S. E. Paulin and B. J. Ackerson, Phys. Rev. Lett. **64**, 2663 (1990).
[21] W. G. Hoover and F. H. Ree, J. Chem. Phys. **49**, 3609 (1968).
[22] Alternatively, one can employ in the same manner the freezing volume fraction, $\phi_f = 0.513$, of a binary mixture having size ratio and composition read from the PSD discussed above [23]. Given the continuous shape of the PSD of the present polymer particles, the true phase behavior probably lies between these two extremes. However, to facilitate comparison with previous work, we identify our suspension with the one-component hard-sphere system for the remainder of this paper. Conversion to the equivalent two-component system is achieved by multiplying the stated volume fractions by the factor $0.513/0.494 = 1.04$.
[23] P. Bartlett, J. Phys.: Condens. Matter **2**, 4979 (1990).
[24] W. van Megen and S. M. Underwood, J. Chem. Phys. **88**, 7841 (1988).
[25] P. N. Pusey, H. M. Fijnaut, and A. Vrij, J. Chem. Phys. **77**, 4270 (1982).
[26] B. R. A. Nijboer and A. Rahman, Physica (Amsterdam) **32**, 415 (1966).
[27] P. N. Pusey and W. van Megen, Physica A **157**, 705 (1989).
[28] J. Z. Xue, D. J. Pine, S. T. Milner, X. L. Wu, and P. M. Chaikin, Phys. Rev. A **46**, 6550 (1992).
[29] J. Müller and T. Palberg, Prog. Colloid Polym. Sci. **100**, 121 (1996).
[30] P. N. Pusey, in *Photon Correlation Spectroscopy and Velocimetry*, edited by H. Z. Cummins and E. R. Pike (Plenum, New York, 1977).
[31] Results shown in Fig. 4 for $\phi = 0.405$ are based on 50 measurements each of 5000 s duration, which, given that the ICF at this volume fraction decays in about 1 s, constitute averages over some 250 000 independent fluctuations of the intensity. About one day was required to obtain the results at $\phi = 0.583$ based on an ensemble of about 4000 independent fluctuations.
[32] P. N. Pusey, J. Phys. A **11**, 119 (1978).
[33] Y. Hiwatari, H. Miyagawa, and T. Odagaki, Solid State Ionics **47**, 179 (1991).
[34] D. Thirumalai and R. D. Mountain, Phys. Rev. E **47**, 479 (1993).
[35] S. Sanyal and A. K. Sood, Phys. Rev. E **57**, 908 (1998).
[36] W. Kob, C. Donati, S. J. Plimpton, P. H. Poole, and S. C. Glotzer, Phys. Rev. Lett. **79**, 2827 (1997).
[37] M. M. Hurley and P. Harrowell, J. Chem. Phys. **105**, 10 521 (1996).
[38] W. van Megen and S. M. Underwood, Phys. Rev. E **47**, 248 (1993).
[39] E. Bartsch, M. Antonietti, W. Schupp, and H. Sillescu, J. Chem. Phys. **97**, 3950 (1992); E. Bartsch, V. Frenz, J. Baschnagel, W. Schärtl, and H. Sillescu, *ibid.* **106**, 3743 (1997).
[40] H. Z. Cummins, G. Li, Y. H. Hwang, G. Q. Shen, W. M. Du, J. Hernendez, and N. J. Toa, Z. Phys. B **103**, 501 (1997).
[41] M. Fuchs, I. Hofacker, and A. Latz, Phys. Rev. A **45**, 898 (1992).
[42] M. Tokuyama, Physica A **229**, 36 (1996); M. Tokuyama, Y. Enomoto, and I. Oppenheim, Phys. Rev. E **56**, 2302 (1997).
[43] M. Fuchs, W. Götze, and M. R. Mayr, Phys. Rev. E **58**, 3384 (1998).
[44] M. Tokuyama and I. Oppenheim, Physica A **216**, 85 (1995).
[45] W. Kob and H. C. Anderson, Phys. Rev. Lett. **73**, 1376 (1994).
[46] F. Speapen and D. Turnbull, Annu. Rev. Phys. Chem. **35**, 241 (1985).
[47] W. van Megen, S. M. Underwood, J. Müller, T. C. Mortensen, S. I. Henderson, J. L. Harland, and P. Francis, Prog. Theor. Phys. Suppl. **126**, 171 (1997).
[48] Q. Broughton, G. H. Gilmer, and K. A. Jackson, Phys. Rev. Lett. **49**, 1496 (1982).
[49] D. J. W. Aastuen, N. A. Clark, L. K. Cotter, and B. J. Ackerson, Phys. Rev. Lett. **57**, 1733 (1986); M. Würth, J. Schwarz, F. Culis, P. Leiderer, and T. Palberg, Phys. Rev. E **52**, 6415 (1995).
[50] J. L. Harland and W. van Megen, Phys. Rev. E **55**, 3054 (1997).
[51] P. Jund, D. Caprion, and R. Jullien, Phys. Rev. Lett. **79**, 91 (1997).